*05*

# The laser prepulse influence on the generation of superstrong magnetic fields in cluster plasma

© *A.A. Andreev*[1,3], *L.A. Litvinov*[1], *K.Yu. Platonov*[2]

[1] St. Petersburg State University, 199034 St. Petersburg, Russia
[2] Peter the Great Saint-Petersburg Polytechnic University, 195251 St. Petersburg, Russia
[3] Ioffe Institute, 194021 St. Petersburg, Russia

e-mail: konstantin_platonov@yahoo.com

The generation of an ultra-strong magnetic field in a cluster plasma in a focal region of an intense circularly polarized laser pulse with a controlled pre-pulse is considered using analytical estimates and numerical modeling. The parameters of the pre-pulse are determined to obtain the maximum amplitude of the quasi-stationary magnetic field.

**Keywords:** intense laser pulse, laser cluster plasma, superstrong magnetic field.

## Introduction

As is known, studies into the methods of generation of superstrong magnetic fields and the influence of such fields on the properties of objects [1] are relevant in various areas of physics and astrophysics. The generation of superstrong magnetic fields and giant magnetic moments based on the excitation of intense circular electron currents in cluster gas targets irradiated by a circularly polarized ultrashort laser pulse of relativistic intensity has been considered in [2–5].

Cluster laser targets are the subject of active current research [6]. To generate a magnetic field, the radii of clusters of such targets should be smaller than the wavelength of laser radiation for circular orbits of electrons to be located outside the ionic cluster core. It was assumed in [2–5] that a short intense laser pulse has no pre-pulse and the density profile of the ionic cluster core is rectangular with a given initial radius (tens and hundreds of nanometers) and solid-state density. In experiments, ultrashort (tens of femtoseconds) laser pulses of relativistic intensity are preceded by a pre-pulse with a duration of tens and hundreds of picoseconds. Modern laser technology can increase the ratio of maximum intensities of a pulse and a pre-pulse, which is called contrast, to a value of $K \leq 10^{10}$ [7], but cannot completely remove it ($K = \infty$). For clusters of small radii and ultrahigh laser intensities ($\leq 10^{22}$ W/cm$^2$), even record-high contrast values leading to a pre-pulse intensity of $< 10^{12}$ W/cm$^2$ can affect the density profile of the plasma cluster [8,9] formed before the arrival of the main pulse. In the worst case of weak contrast, clusters will have time to heat up and expand to a transparent state (the density will fall below the critical density) before the arrival of the main pulse, which will reduce its absorption and the associated momentum transfer from laser radiation to electrons. The absorption coefficient (actually, the coefficient of momentum transfer from circularly polarized radiation to electrons) depends on the density and radius of the cluster; therefore, it is possible to achieve maximum absorption and maximum strength of the generated magnetic field by setting the right pre-pulse parameters (intensity and duration).

In the present work, analytical and numerical studies of the influence of pre-pulse parameters on the density profile of the gas target cluster, on the absorption coefficient of cluster plasma, and on the strength of the generated quasi-stationary magnetic field have been carried out. The optimal parameters of the target were determined with account for the contrast value of an intense laser pulse.

## Influence of a laser pre-pulse on a cluster

Consider a spherical target of constant mass that is first exposed to a pre-pulse with intensity $I_{Lp}$ and duration $t_{Lp}$ and then to a main pulse with intensity $I = KI_{Lp}$ at contrast $K$. The initial ion concentration of the target plasma is chosen to be close to solid-state value $n_{i0} = 6 \cdot 10^{22}$ cm$^{-3}$, and the initial density profile is rectangular. The collision mechanism [10] of absorption of the laser pre-pulse by plasma is dominant in this case. Numerical modelling of the interaction of a gold cluster with pre-pulses of varying intensity ($10^{12} - 10^{13}$ W/cm$^2$) and duration ($4 - 20$ ps) was carried out using the hydrodynamic code [11]. The electron temperature was $T_{eLp} \geq 5$ eV within the entire range of pre-pulse parameters, and plasma expanded at a velocity close to ion sound velocity $c_s \approx \sqrt{Z_{Lp}T_{eLp}/m_i} \geq 2 \cdot 10^5$ cm/s, where $m_i$ and $Z_{Lp}$ are the mass and charge of an ion. The maximum $n_{i\,\max}$ density of the target decreased with time upon expansion in accordance with the condition of target

mass conservation:

$$n_{i\,\mathrm{max}}(t) \approx n_{i0}[R_{i0}/(R_{i0} + c_s t)]^3.$$

Since a relatively short pre-pulse was used, the plasma ion charge was determined via the probability (per unit time) of tunneling ionization of a target atom in the electric field of the laser wave [12]. The obtained average value $Z_{Lp} \sim 2$ for the ion charge was used in further calculations. After interaction with the pre-pulse, the density profile of the target was close to a trapezoid with density gradient $l_{\mathrm{fr}} = \alpha c_s t_{Lp}$ ($\alpha \leq 1$) and maximum density $n_{i\,\mathrm{max}} = n_{i0}[R_{i0}/(R_{i0} + c_s t_{Lp})]^3$. Hydrodynamic calculations have shown that at various absorption coefficients ($\eta_{Lp} < 0.8$) of laser pre-pulse radiation, a less than 20% expansion of a 100 nm Au cluster (i.e., a 20% increase in radius and a corresponding decrease in density) is achieved at a pre-pulse intensity $\leq 10^{12}\,\mathrm{W/cm}^2$ and a duration $\leq 8$ ps. Further 3D calculations of the interaction between the cluster and the main pulse performed using the PIC code EPOCH [13] showed that such cluster dispersal does not affect the magnitude of the generated magnetic field, and pre-pulses with parameters satisfying the $I_{Lp} t_{Lp} \leq 8 \cdot 10^{12}\,\mathrm{W \cdot ps/cm^2}$ condition do not affect the subsequent interaction of submicron gold clusters with the main pulse. If this condition is violated, the radius of the cluster grows, the density drops, and the pre-pulse starts to affect the strength of the generated magnetic field.

To quantitatively describe this influence in the analytical model, we will consider the plasma density profile of the cluster formed under the action of the laser pre-pulse, first in the shape of a rectangle of varying width $2R_0$ and height $n_i$ with a constant mass when $n_{i0} = n_{i0}[R_{i0}/R_0]^3$. Note that the replacement of the trapezoidal profile by a rectangular one is justified by the considered small initial radii of the cluster ($R_{i0} \sim 100$ nm), since the density already falls below the critical one upon expansion to $R_0 \sim 5R_{i0}$ and the absorption decreases significantly, which is not optimal for the generation of the magnetic field. Accordingly, the scale of the sloping parts of the trapezoid in the considered range will be smaller than the laser wavelength, and the trapezoidal density profile can be replaced by a radially averaged rectangular profile.

Under the influence of the pre-pulse, the cluster is ionized and heated, and a certain fraction of electrons leave the cluster. As a result, the cluster becomes charged. Using the relations for cluster charge $Q_{Lp}$ at a given pre-pulse field strength $E_{Lp} = \sqrt{4\pi I_{Lp}/c}$ given in [14], we obtain that the charge for an $R_{i0} = 100$ nm cluster of solid-state density at $L_{Lp} = 10^{12}\,\mathrm{W/cm^2}$ is very small,

$$k = 3Q_{Lp}/4\pi Z_{Lp} e n_{i0} R_{i0}^3 \approx 2 \cdot 10^{-4},$$

relative to the charge of the ionic core. Temperature $T_{eLp}$ of cluster heating by the pre-pulse can be estimated by the formula [15]

$$T_{eLp} \approx \frac{m_i}{Z_{Lp}} \left( \frac{\eta_{Lp} I_{Lp}}{\rho_0} \right)^{2/3},$$

where $\rho_0$ is the initial target density and $\eta_{Lp}$ is the pre-pulse collisional absorption coefficient. We obtain $T_{eLp} \sim 50\,\mathrm{eV}$ and gold ion velocity $v_i = \sqrt{Z_{eLp} T_{eLp}/m_i} \approx 5 \cdot 10^5\,\mathrm{cm/s}$ for an $\mathrm{Au}^{+2}$ target with a solid-state density at $I_{Lp} = 10^{12}\,\mathrm{W/cm^2}$ and $\eta_{Lp} \approx 0.2$. Under the action of Coulomb forces and thermal pressure, the cluster disperses during a pre-pulse.

An analytical model of the heated charged cluster dispersal is constructed in the Appendix. This model makes it possible to estimate radius $R_0(t_{Lp})$ and electron density $n_e(t_{Lp})$ at the end of the pre-pulse and to use these estimates for further modelling of the interaction of the partially dispersed cluster with the main laser pulse. Figure 1 shows the dependence of radius $R_0$ and density $n_e$ on pre-pulse duration $t_{Lp}$ for a gold cluster of radius $R_{i0} = 100$ nm under the influence of a $10^{12}$ W/cm$^2$ pre-pulse at cluster expansion velocity $c_{sQ} = 5 \cdot 10^5$ cm/s plotted by formula (A5). Figure 1 demonstrates that by varying the duration of the pre-pulse, electron density $n_e(t_{Lp})$ of the cluster can be varied over a wide range from a characteristic solid-state value of $6 \cdot 10^{22}\,\mathrm{cm^{-3}}$ to transparency threshold $n_{cr} \approx 10^{21}\,\mathrm{cm^{-3}}$ for radiation with wavelength $\lambda_L \sim 1\,\mu\mathrm{m}$.

## Absorption of the main circularly polarized laser pulse by the cluster

The magnetic field strength [16] generated by the main pulse depends on intensity $I$ of the main laser pulse, its duration $\tau_L$, cluster radius $R_0(t_{Lp})$, and absorption coefficient $\eta$, which, in turn, depends on density $n_e(t_{\mathrm{LP}})$. Coefficient $\eta$ of absorption of linearly polarized radiation by a nanocluster was considered in [10,17–19]. The main mechanism of absorption of an intense laser pulse by a cluster is resonant collisionless absorption [17]. It is known that when the electrons of a cluster with density $n_e(t_{Lp})$ are displaced relative to the ionic core, a restoring ambipolar field arises between the electron shell and the ionic core, resulting in oscillations of the electron shell relative to the ionic core under the influence of the electric field of the laser wave. The vibrational process has a resonant character, and the amplitude of electron oscillations and the laser field energy absorbed by the cluster increase when laser wave frequency $\omega$ matches natural frequency $\omega_{pe}/\sqrt{3}$ ($\omega_{pe}^2 = 4\pi e^2 n_e(t_{Lp})/m_e$ is the plasma frequency of cluster electrons) of oscillations of the spherical electron shell. Resonance condition $\omega = \omega_{pe}/\sqrt{3}$ can be fulfilled because the cluster density decrease shown in Fig. 1 starts already during a laser pre-pulse, and ratio $\omega_p/\omega \sim 10\sqrt{Z}$, which is valid for solid-state values of electron concentration under the influence of the pre-pulse, falls down to the resonance value of $\omega_p/\omega \sim \sqrt{3}$. Choosing the right pre-pulse duration $t_{Lp}$ and its intensity $I_{Lp}$ in formulae (A5), one can obtain the resonance value of the cluster density

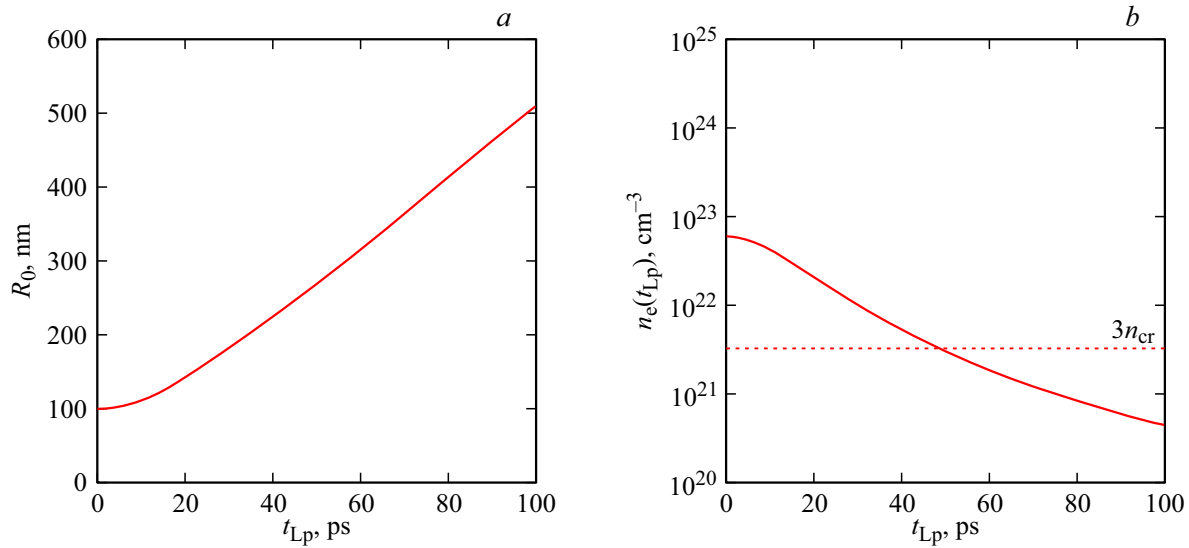$$n_e(t_{Lp}) = 3m_e \omega^2 / 4\pi e^2 = 3n_{cr}$$

**Figure 1.** Dependences of (*a*) radius $R_0$ (in nm) and (*b*) density $n_e$ (in cm$^{-3}$) on pre-pulse duration $t_{Lp}$ (in ps) for an Au$^{+1}$ cluster with initial radius $R_{10} = 100$ nm under the influence of a pre-pulse with intensity $I_{Lp} = 10^{12}$ W/cm$^2$ ($c_{sQ} = 5 \cdot 10^5$ cm/s).

(dashed horizontal line in Fig. 1, *b*) for the rectangular density profile. In [10], the linearized motion equation of a cluster electron was used to obtain absorption coefficient

$$\eta_l(n_e(t_{Lp})) = \eta_{\max} \frac{\Gamma_s}{(\omega_{pe}^2/\omega^2 - 3)^2 + \Gamma_s}, \quad \Gamma_s = 9 \frac{\nu_{ei}\omega_{pe}}{2\omega^2}, \tag{1}$$

which reaches its maximum value $\eta_{\max}$ at resonance frequency $\omega = \omega_{pe}/\sqrt{3}$. The half-width of the frequency distribution of the absorption coefficient is determined by frequency $\nu_{ei}$ of electron-ion collisions leading to dissipation of the energy absorbed by electrons.

Absorption coefficient (1) was obtained using the linearized equations of electron motion under the assumption that the dimensionless amplitude of the laser field is small: $a_0 = eE_0/m_e\omega c \ll 1$. The generation of superstrong magnetic fields requires laser fields of ultrarelativistic strength ($a_0 \gg 1$) where formula (1) for the absorption coefficient needs to be modified. At high temperature $T_e$ of cluster electrons during a main pulse, the collision frequency ($\nu_{ei} \sim T_e^{-3/2}$) decreases rapidly, the collisional absorption becomes weak, and the resonance in formula (1) is narrow. It was demonstrated in [17] that for short (several periods) laser pulses, the time profile of the pulse envelope must be taken into account in the equation of electron motion. The field of a real laser pulse wave also has a quadratic correction to the wave phase: $\omega \to \omega + \dot\omega t$. With finite pulse duration $\tau_L$, $\omega$ [17]

$$\omega_{pe}^2(a_0) = 4\pi e^2 n_e(t_{Lp})/\gamma m_e.$$

Resonance at the laser pulse frequency at a certain cluster density and laser field strength $a_0$ ($\omega = \omega_{pe}(a_0)/\sqrt{3}$) should remain, but in the relativistic case an additional resonance is possible at the doubled laser frequency ($2\omega = \omega_{pe}/\sqrt{3}$) with which the ponderomotive pressure

force changes. Depending on the width of the resonance ($\nu_{eff} \ll \omega$, $\nu_{eff} \gg \omega$), resonances may appear individually or merge into one. In addition to the resonant absorption mechanism, an absorption mechanism similar to the Brunel [20,21] one, which adds term $\eta_0$ to the resonant absorption coefficient, operates for a cluster with a sharp boundary and a high initial density. With this in mind, total absorption coefficient of the cluster $\eta_\Sigma$ in the case of relativistic laser field strengths can be written in the following form:

$$\eta_\Sigma(n_e(t_{Lp}); I) \approx \eta_0(n_e; I) + \eta_{\max}(n_e; I) \frac{\Gamma_n}{(\omega_{pe}^2/\omega^2 - \mu)^2 + \Gamma_n},$$

$$\Gamma_n = 9 \frac{\nu_{eff}(n_e; I)\omega_{pe}}{2\omega^2},$$

$$\omega_{pe}^2 = 4\pi n_e(t_{Lp})e^2/\gamma m_e, \quad 3 \le \mu \le 12. \tag{2}$$

Here, the values of $\eta_0(n_e; I)$, $\eta_{\max}(n_e; I)$, and $\nu_{eff}(n_e; I)$ are determined using the standard power-law dependence:

$$\eta_{0,\max}(n_e; I) = \eta_{0,\max}(n_{en})^{\alpha_{1,3}}(I_n)^{\alpha_{2,4}},$$

$$\nu_{eff}(n_e; I) = \nu_{eff}(n_{en})^{\alpha_5}(I_n)^{\alpha_6},$$

$$I_n = \frac{I}{10^{20}\,\text{W/cm}^2}, \quad n_{en} = \frac{n_e}{Z \cdot 3 \cdot 10^{22}\,\text{cm}^{-3}},$$

$$10^{21}\,\text{cm}^{-3} < n_e < 10^{24}\,\text{cm}^{-3}, \quad 0.1 < I_n < 10^3, \tag{3}$$

where constants $\eta_0$, $\eta_{\max}$, $\nu_{eff}/\omega$ and exponents of power $\alpha_1 - \alpha_6$ are determined from numerical simulation data.

Figure 2 shows the data of numerical simulation of the dependence of the absorption coefficient of an Au$^{+30}$ cluster of radius $R_0 = 200$ nm on its initial ion density $n_i = n_e/Z$ ($Z = 30$) and laser intensity $I$. Figure 2, *b* confirms the conservation of the absorption character resonant in
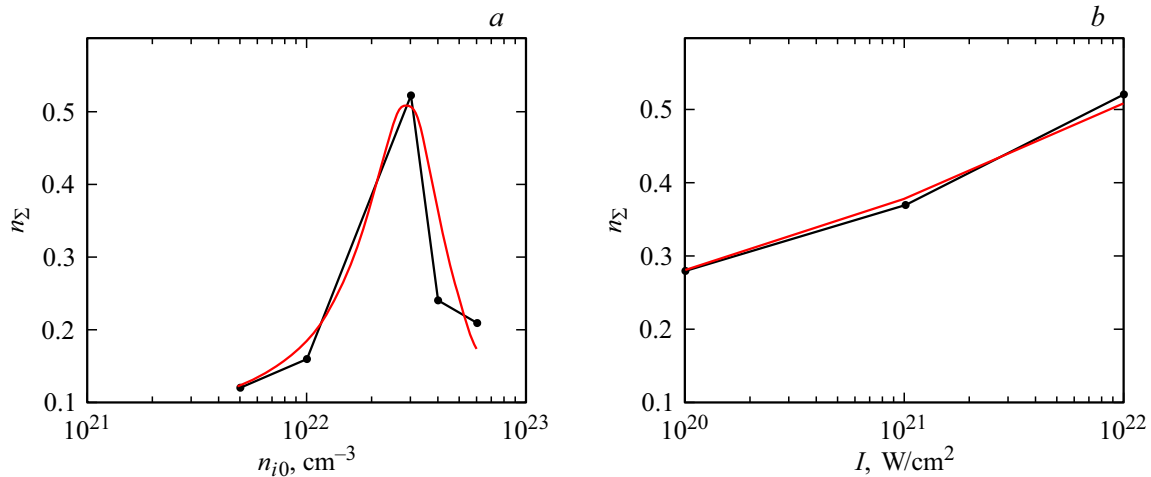
**Figure 2.** (*a*) Cluster absorption coefficient as a function of the initial ion cluster density at $I = 10^{22}$ W/cm$^2$ and $R = 200$ nm. (*b*) Cluster absorption coefficient as a function of the peak laser pulse intensity at $n_{i0} = 3 \cdot 10^{22}$ cm$^{-3}$ and $R = 200$ nm. Black dots — numerical modelling. Red lines — formula (3).

cluster density in the ultrarelativistic case ($a_0 \approx 85$ at $I = 10^{22}$ W/cm$^2$). Red theoretical curves *2* in Fig. 2 correspond to the following power scaling parameters: $\eta_0 = 0.11$, $\mu = 9$, $\eta_{\max} = 0.4$, $\alpha_{1,2,3,5,6} = 0$, $\alpha_1 = 0.13$, and $\nu_{eff}/\omega = 2.5$. Significant values of effective collision frequency $\nu_{eff}/\omega = 2.5$ and $\mu = 9$ correspond to merging of the ordinary and ponderomotive resonances into one and to preservation of a single absorption coefficient maximum over the cluster density in the ultrarelativistic case.

## Magnetic field of the cluster

In study [16] the dynamics of the electron shell of a cluster was examined in detail, and it was shown that the amplitude of magnetic field $H$ of a single cluster grows linearly with time within the main laser pulse, reaching its maximum by the time of its termination:

$$\frac{H(t)}{E_0} \approx \frac{\eta_\Sigma a_0 c t}{4 r_E (1 + a_0^2)^{1/2}}, \quad t \in [0; \tau_L]. \quad (4)$$

Here, $\eta_\Sigma$ is the absorption coefficient of the main pulse shown in Fig. 2, while the characteristic radius of electron orbits in the cluster in (4) is estimated as $r_E = C R_0$, where $C \approx 3$. A more precise value ($2 \leq C \leq 5$) is determined by numerical modelling and depends on the laser intensity and the radius and density of a cluster. In order for electrons to be retained by the ionic cluster core, charge $Q$ of the cluster resulting from partial extraction of electrons by the main laser pulse must satisfy inequality

$$m_e c^2 \left( \sqrt{1 + a_0^2} - 1 \right) < \frac{eQ}{r_E}$$

(the kinetic energy is lower than the potential energy). The magnitude of charge $Q$ increases with increasing laser intensity as $\sqrt{I}$ and cannot exceed the total charge

of the ionic cluster core ($4\pi R_{i0}^3 Z e n_{i0}/3$). As a result, dimensionless amplitude $a_0$ of the laser field must satisfy condition [4]

$$a_0 < a_{tr} \approx \frac{4\pi \eta_\Sigma e^2 \omega}{9 m_e c^3} Z n_i R_0^3 > 1.$$

When the value of $a_{tr}$ is exceeded, the magnetic field of the cluster will start to decrease rapidly with increasing $a_0$, since the ionic core is unable to retain all the electrons absorbing laser energy in finite orbits. Note that the threshold laser field differs from the field required for „Coulomb explosion" of the cluster (complete removal of electrons from the cluster)

$$a_{Ql} \approx \frac{2}{3} Z n_{i0} e^2 R_{i0} \lambda / m_e c^2.$$

Ratio $a_{tr}/a_{Ql} \approx 4\pi^2 \eta_\Sigma R_0^2/3\lambda^2 < 1$ at $R_0 < \lambda$. After termination of the laser pulse ($t > \tau_L$), the magnetic field begins to decrease with time due to the adiabatic dispersal of the cluster heated by the main pulse [4]:

$$H(t) = H(\tau_L)(R_0/R(t))^3,$$

$$R(t) \approx \sqrt{R_0^2 + Z m_e c^2 (t - \tau_L)^2 ((1 + a_0^2)^{1/2} - 1/m_I)}, \quad t \geq \tau_L. \quad (5)$$

Since $\eta_\Sigma$ and $R_0$ are determined by pre-pulse parameters, estimate (4) of the magnetic field of the cluster also depends on the pre-pulse parameters via the value of electron density $n_e(t_{Lp})$ (ion density $n_i(t_{Lp}) = n_e(t_{Lp})/Z$) at the end of the pre-pulse.

The red curve in Fig. 3 represents dependence (5) of magnetic field amplitude $H(\tau_L)$ of a cluster with $R_{i0} = 200$ nm on ion density $n_i(t_{Lp})$ at the moment of pre-pulse termination for intensity $I = 10^{22}$ W/cm $^2$ of the main laser pulse. Figure 3 shows that the density-resonant nature of the absorption coefficient in Fig. 2 leads to a
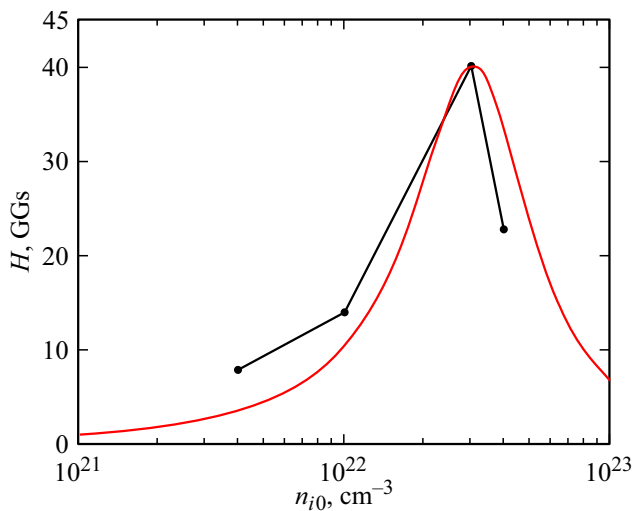
**Figure 3.** Maximum of the quasi-stationary magnetic field as a function of the initial ion density $n_I = n_e(t_{Lp})/Z_{Lp}$ of the cluster at $I = 10^{22}\,\text{W/cm}^2$ and $R = 200\,\text{nm}$. Black dots — PIC calculation. Red curve — analytical dependence (5) with absorption coefficient (4).

similar dependence of the magnetic field amplitude. Since plasma resonance is achieved with the considered laser intensities at an ion density of $3 \cdot 10^{22}\,\text{cm}^{-3}$, which is close to the initial cluster density of $5.9 \cdot 10^{22}\,\text{cm}^{-3}$, the radius increase required to reach the resonance density is small: $R_0 = R_{i0}(5.9/3)^{1/3}$. Effective radius $r_\Sigma = CR_0$ of the electron orbit in formula (4) remains practically unchanged in the vicinity of the resonance density, and the density dependence of the magnetic field practically matches the density dependence of absorption coefficient (2). Note that the maximum quasi-stationary magnetic field with an amplitude of 40 GGs is significantly stronger than the magnetic field of the laser wave (6.5 GGs) corresponding to a laser intensity of $10^{22}\,\text{W/cm}^2$.

In order to verify the analytical estimates of the absorption coefficient and magnetic field and determine scaling constants $\eta_{\max}(n_e; I)$, $\nu_{eff}(n_e; I)$, we performed 3D PIC modelling (code EPOCH [13]) of dispersal of $\text{Au}^{+30}$ clusters with radii of 50, 100, and 200 nm irradiated with a 10 fs circularly polarized laser pulse in the intensity range from $10^{20}$ to $10^{22}\,\text{W/cm}^2$ propagating along axis $x$. The cluster was located in the center of the simulation box: $x = y = z = 0$. The dimensions of the simulation box were $4 \times 4 \times 4\,\mu\text{m}$. It was divided into $400 \times 400 \times 400$ cells along axes $x, y$, and $z$, and the maximum number of particles per cell was 200 for electrons and 40 for ions. Cluster expansion under the influence of the pre-pulse was accounted for by the initial value of the ion density of the cluster, which varied from $6 \cdot 10^{22}\,\text{cm}^{-3}$ (no pre-pulse, solid-state density of the target) to IFx154x cm$^{-3}$ (cluster dispersed during the pre-pulse).

Figure 3 shows the dependence of magnitude (in simulation space and time) of the quasi-stationary magnetic field

on the initial ion density of the cluster at $I = 10^{22}\,\text{W/cm}^2$ and $R_{0i} = 200\,\text{nm}$. The obtained simulation results reveal the presence of an optimum of the ion density with respect to the maximum value of the generated magnetic field. Optimum density $n_i^* \approx 3 \cdot 10^{22}\,\text{cm}^{-3}$ (at a laser intensity of $10^{22}\,\text{W/cm}^2$) corresponds to plasma frequency

$$\omega_{pe}^2 = 4\pi Z n_i^* e^2/m_e(1 + a_0^2)^{1/2}$$

of cluster electrons that falls within the $3\omega^2 < \omega_{pe}^2 < 12\omega^2$ resonance interval of the electric field and ponderomotive pressure forces. A combination of the absorption peaks of conventional and ponderomotive resonances is the broad peak of Fig. 3.

Since the plasma frequency in resonant absorption coefficient (2) depends on ratio $n_e(t_{Lp})/a_0 \sim n_e(t_{Lp})/\sqrt{I}$, the magnetic field amplitude depends in similar ways both on density and on laser intensity. The latter dependence is plotted in Fig. 4 in accordance with formula (4) for a fixed cluster density of $6 \cdot 10^{22}\,\text{cm}^{-3}$ and cluster radii of 50 (blue curve) and 200 nm (red curve). Vertical dashed lines show the threshold intensities corresponding to the cluster radii (corresponding to amplitude $a_{tr}$) above which formula (4) becomes inapplicable. Black and green dots show the PIC modelling data. Magnetic fields with strengths in the tens of GGs in Figs. 3 and 4 lead to magnetization and an increased ion density in the inner area of the cluster. Figure 5 shows the ion density distribution for a 200 nm cluster with density $n_i = 6 \cdot 10^{22}\,\text{cm}^{-3}$ at a laser intensity of $10^{22}\,\text{W/cm}^2$ when, according to Fig. 4, a magnetic field with a maximum amplitude of $\sim 15\,\text{GGs}$ is generated. A spindle-shaped region, where the ion density reaches a value of $2 \cdot 10^{23}\,\text{cm}^{-3}$ at an initial density of $6 \cdot 10^{22}\,\text{cm}^{-3}$, is seen at the center of the cluster with a radius of 200 nm. This
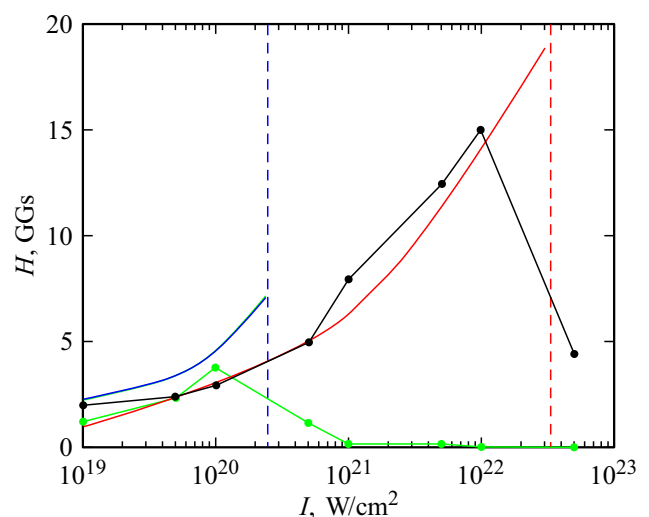


**Figure 4.** Maximum magnetic field (5) as a function of the intensity of the main laser pulse at $R = 200\,\text{nm}$ (red line) and $R = 50\,\text{nm}$ (blue line). Density $n_i = 6 \cdot 10^{22}\,\text{cm}^{-3}$. Black circles — PIC calculation for a radius of 200 nm; green circles — for 50 nm. Vertical dashed lines show the thresholds corresponding to limiting amplitude $a_{tr}$ of clusters with radii of 50 and 200 nm.
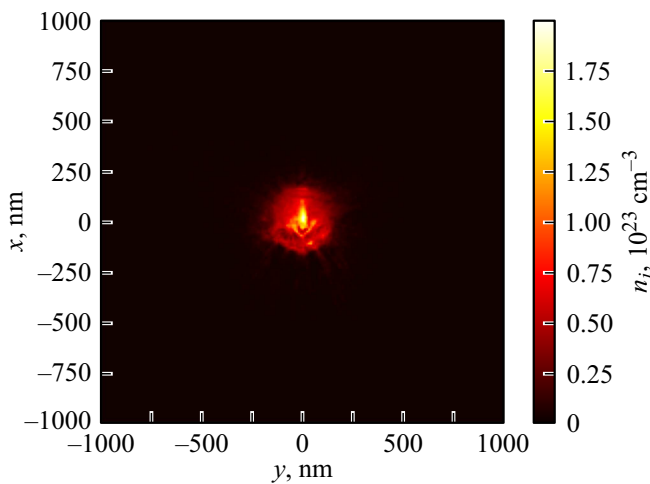
**Figure 5.** Ion density in the $xy$ plane (laser radiation propagates along axis $x$) and the diametral section ($z = 0$) of the cluster at the end of the laser pulse at $R = 200$ nm, $n_i = 6 \cdot 10^{22}$ cm$^{-3}$, $I = 10^{22}$ W/cm$^2$.



**Figure 6.** Quasi-stationary magnetic field as a function of the scale of inhomogeneity of the trapezoidal cluster density profile. The number of particles is constant and corresponds to the number of particles for the rectangular profile at $R_0 = 200$ nm, the black curve corresponds to $n_i = 3 \cdot 10^{22}$ cm$^{-3}$, and the blue curve corresponds to $n_i = 6 \cdot 10^{22}$ cm$^{-3}$. The red lines correspond to analytical model (5), (7). $I = 10^{22}$ W/cm$^2$.

increase in density is explained by magnetic compression of the central area of the cluster.

Thus, the numerical simulation confirms theoretical estimates of high cluster absorption. When constants of the analytical model are calibrated against numerical data, the model agrees well with the numerical dependences of the magnetic field amplitude on the parameters of the cluster and the laser pulse.

To verify the correctness of using a rectangular cluster density profile, magnetic field amplitude modelling was carried out for a cluster with a trapezoidal ion density profile:

$$n_i(r) = \begin{cases} n_i(R_0 - r)/L & R_0 - L \leq r \leq R_0, \\ n_i, & 0 \leq r \leq R_0 - L \end{cases},$$

(see Fig. 6). It follows from Fig. 6 that for resonance ion density $n_i = 3 \cdot 10^{22}$ cm$^{-3}$, blurring of the cluster boundaries reduces the absorption coefficient and magnetic field strength, since the resonance condition is not satisfied in the emerging regions of lower density. However, as the behavior of the black curve in Fig. 6 suggests, inhomogeneity scale $L$ must be greater than one half of the initial cluster radius for the reduction effect to manifest itself. At $L < 0.3R$), the spatial inhomogeneity of density does not noticeably affect the magnetic field magnitude even in the resonant case. At a contrast of $10^{10}$ (a pre-pulse intensity of $10^{12}$ W/cm$^2$ with a main pulse intensity of $10^{22}$ W/cm$^2$), this scale of inhomogeneity in hydrodynamic modelling is found at a pre-pulse duration of $\sim 10$ ps. In the absence of resonance (blue curve in Fig. 6), the influence of the density gradient on the magnitude of the magnetic field is practically zero up to $L \sim R_0$. An analytical estimate of the dependence of the absorption coefficient and the magnetic field on the scale of inhomogeneity can be derived from formula (2) if
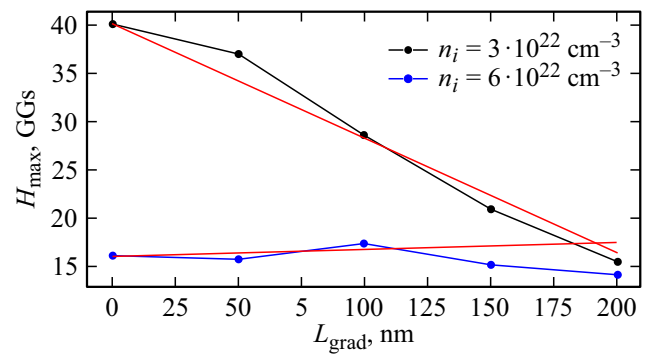
the plasma frequency of electrons becomes a function of $r$, $\omega_{pe} \to \omega_{pe}(r)$. Averaging over $r$ according to the formula

$$\langle \eta_\Sigma \rangle = R_0^{-1} \int_0^{R_0} \eta_\Sigma(r) dr,$$

one may then obtain an analytical dependence of the absorption coefficient on the scale of inhomogeneity of the ion density:

$$\langle \eta_\Sigma(n_e(t_{Lp}); I; L) \rangle \approx \eta_0(n_e; I) + (1 - L/R_0)\eta_{\max}(n_e; I)$$

$$\times \frac{9\frac{v_{eff}(n_e;I)\omega_{pe}}{2\omega^2}}{(\omega_{pe}^2/\omega^2 - \mu)^2 + 9\frac{v_{eff}(n_e;I)\omega_{pe}}{2\omega^2}} + \frac{3L\omega v_{eff}^{1/2}(n_e;I)}{\sqrt{2}R_0\omega_{pe}^{3/2}}$$

$$\times \left[ \text{arctg} \frac{\sqrt{2}\omega(\omega_{pe}^2/\omega^2 - \mu)}{3v_{eff}^{1/2}(n_e;I)\omega_{pe}^{1/2}} + \text{arctg} \frac{\sqrt{2}\omega\mu}{3v_{eff}^{1/2}(n_e;I)\omega_{pe}^{1/2}} \right].$$

$$(6)$$

Formula (4) with absorption coefficient (6) allows us to construct the analytical dependence of the magnetic field amplitude on the scale of inhomogeneity, which is shown in Fig. 6 with red lines for a resonant density of $3 \cdot 10^{22}$ cm$^{-3}$ and an above-resonant density of $6 \cdot 10^{22}$ cm$^{-3}$. Comparison of the resonant and non-resonant density values in Fig. 6 shows that the absorption at a cluster density higher than the resonant density cannot be increased noticeably by blurring the boundary and obtaining a local resonant density value: this local area is too small compared to the full volume of the cluster.

Summarizing the numerical and analytical simulations, one may note that, according to (4), it is necessary to increase laser field strength $a_0$ and absorption coefficient $\eta_\Sigma$ in order to achieve the maximum magnetic field amplitude. For a given cluster radius in formula (4), there is a limit ($a_{tr}$) to the growth of intensity $a_0$ of the laser field and duration $\tau_L$ of the laser pulse (characteristic radius $r_E$

of electron orbits should not change appreciably within the pulse duration). Putting these requirements together, we obtain estimates of the optimal target parameters for generation of superstrong magnetic fields with account for the contrast of an intense laser pulse:

$$\frac{n_e(t_{Lp})}{n_{cr}} \approx 9a_0 = 9\left(\frac{I\lambda^2}{1.37 \cdot 10^{18}\,\text{W}(\mu\text{m}^2/\text{cm}^2)}\right)^{1/2},$$

$$I > 10^{18}\,\text{W/cm}^2. \quad a_0 \approx \eta_\Sigma \frac{n_e(t_{Lp})}{9n_{cr}}\left(\frac{2\pi R_0}{\lambda}\right)^3,$$

$$\frac{c\tau_L}{R_0(t_{Lp})} \approx 4\left(\frac{m_i}{Zm_e a_0}\right)^{1/2}, \quad a_0 \gg 1, \quad L < 0.3R_0. \quad (7)$$

A comparison of the 1st and 2nd lines of conditions (7) shows that there exists an optimal cluster radius $R_0^* \approx \eta_\Sigma^{-1/3}\lambda/2\pi$. For the maximum value of the absorption coefficient (in Fig. 2, *a*) and a wavelength of $1\,\mu\text{m}$, the optimal radius is $R_0^* \approx 200\,\text{nm}$. To obtain optimal cluster density $n_e(t_{Lp}) \approx 9a_0 n_{cr}$, duration $t_{Lp}$ of the pre-pulse and its intensity $I_{Lp}$ in condition (7) must satisfy the following relation:

$$\left(\frac{I\lambda^2}{1.37 \cdot 10^{18}\,\text{W}(\mu\text{m}^2/\text{cm}^2)}\right)^{1/2}$$

$$\times \left(1 + 6\left(\frac{\eta_{Lp}I_{Lp}}{\rho_0}\right)^{2/3}\frac{t_{Lp}^2}{R_{i0}^2}\right)^{3/2} \approx \frac{Zn_{i0}}{9n_{cr}}. \quad (8)$$

It can also be noted that the resonance density and an increased field amplitude are obtained not only by reducing the density due to the pre-pulse, but also by artificially reducing the density of (porous) matter and setting the maximum degree of ionization of cluster atoms. This will be the subject of future study.

## Conclusion

In the present work, the effect of a laser pre-pulse on the generation of a quasi-stationary magnetic field with its strength up to several tens of GGs existing in the focal waist of an ultrahigh-power short laser pulse was considered. The effect of a high-contrast pre-pulse (not accompanied by a significant change in cluster density) is negligible. Lowering of the contrast (increase in the intensity and duration of the pre-pulse) leads to cluster expansion, a decrease in its density, and the emergence of resonance between the plasma frequency of cluster electrons and the laser frequency. Resonance leads to a significant (several-fold) increase in absorption of the angular momentum of circularly polarized laser radiation and, consequently, to an increase in the angular momentum, magnetic moment, and magnetic field generated by rotating electrons of the cluster. The magnetic field increases several times compared to a cluster of a solid-state density and reaches an amplitude of tens of GGs at a laser intensity of $10^{22}\,\text{W/cm}^2$, which is
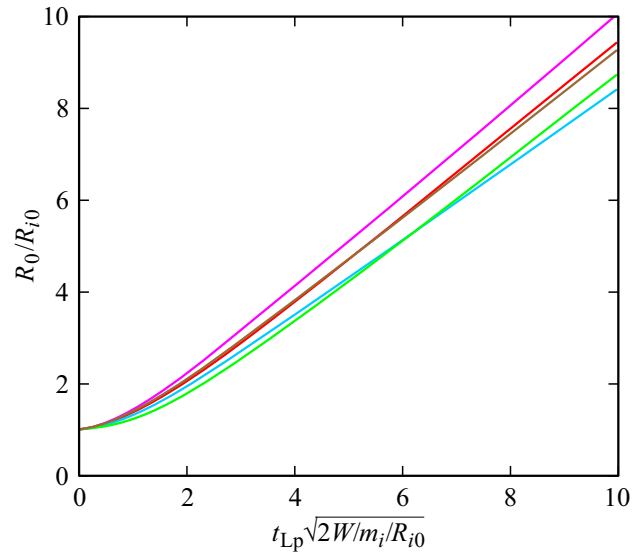


**Figure 7.** Dependence of dimensionless cluster radius $R_0/R_{i0}$ on dimensionless pre-pulse duration $t_{Lp}\sqrt{2W/m_i}/R_{i0}$ plotted using exact formula (A2) — blue, red, and green curves for $\varepsilon = 0, 0.5, 1$. The same dependence plotted using approximation (A5) — lilac, brown, and blue curves for $\varepsilon = 0, 0.5, 1$.

several times higher than the laser field amplitude. Thus, at given laser pulse parameters, there is an optimal density for generation of the magnetic field of maximum amplitude. This density may be achieved by adjusting the intensity and duration (contrast) of the pre-pulse. A density gradient with a scale smaller than $\sim 30\%$ of the cluster radius does not affect the magnetic field amplitude.

## Conflict of interest

The authors declare that they have no conflict of interest.

## Appendix

The law of conservation of energy (integral of the equation of motion of an ion at the outer boundary of the cluster) under the action of thermal and Coulomb forces is as follows:

$$\frac{m_i}{2}\left(\frac{dR_0}{dt}\right)^2 + \frac{3Z_{Lp}T_{eLp}(1-k)R_{i0}^2}{R_0^2}$$

$$+ \frac{Z_{Lp}eQ}{R_0} = 3Z_{Lp}T_{eLp}(1-k) + \frac{Z_{Lp}eQ}{R_{i0}}. \quad (A1)$$

In [19], the interaction energy of the ion with the formed electron shell of a cluster is also introduced into (A1), yielding an additional term $Q(R_0^2 - R_{i0}^2)/R_0^3$ in the left-hand part of (A1). In the present case, because of the smallness of $k$ and the Debye radius of electrons with temperature $T_{rLp}$, the influence of electrons is accounted for by the thermal $(\sim T_{eLp})$ term in (A1). The parametric solution of Eq. (A1) has the form

$$R(\xi) = R_{i0}\big(\varepsilon/2 + (1 - \varepsilon/2)\operatorname{ch}\xi\big), \ \ \xi \in [0; \infty[,$$

$$t(\xi) = \frac{R_{i0}}{\sqrt{2W/m_I}}\big((1 - \varepsilon/2)\operatorname{sh}\xi + \varepsilon\xi/2\big),$$

$$W = 3Z_{Lp}T_{eLp}(1 - k) + \frac{ZeQ}{R_{i0}}, \ \ \varepsilon = ZeQ/WR_{i0}. \quad \text{(A2)}$$

Parameter $0 \le \varepsilon \le 1$ in (A2) characterizes the relationship between Coulomb and thermal forces that accelerate the outer boundary of the cluster. When thermal forces $(\varepsilon = 0)$ are dominant, it follows from (A2) that

$$R_) = \sqrt{R_{i0}^2 + c_s^2 t_{Lp}^2}, \ \ c_s = \sqrt{6Z_{Lp}T_{eLp}(1 - k)/m_i},$$

$$3T_{eLp}(1 - k) \gg eQ/R_{i0}. \quad \text{(A3)}$$

When Coulomb forces $\big(\varepsilon = 1$ in (A2)$\big)$ predominate, it follows from (A2) that

$$R(\xi) = R_{i0}\operatorname{ch}^2\xi,$$

$$t_{Lp}(\xi) = \sqrt{\frac{m_{OI}R_{i0}^3}{8Z_{Lp}eQ}}\big(2\xi + \operatorname{sh}(2\xi)\big), \ \ \xi \in [0; \infty[,$$

$$3T_{eLp}(1 - k) \ll eQ/R_{i0}. \quad \text{(A4)}$$

For practical estimates of the dependence of the cluster radius on the duration of the pre-pulse within the $R_{i0} \le R_) \le 10R_{i0}$ interval, it is convenient to use a simple approximation of parametric dependence (A2):

$$R_0(t_{Lp}) \approx \sqrt{R_{i0}^2 + 2(1 - 0.3\varepsilon)Wt_{Lp}^2/m_i},$$

$$n_e(t_{Lp}) = Z_{Lp}n_{i0}\left(\frac{R_{i0}}{R_0(T_{Lp})}\right)^3. \quad \text{(A5)}$$

Figure 7 shows a comparison of the dependencies of dimensionless radius $R_0/R_{i0}$ on dimensionless pre-pulse duration $t_{Lp}\sqrt{2W/m_i}/R_{i0}$ plotted using exact formula (A2) (blue, red, and green curves for $\varepsilon = 0, 0.5, 1$) and approximation (A5) (lilac, brown, and blue curves for $\varepsilon = 0, 0.5, 1$). The accuracy of approximation (A5) is sufficient to estimate the rate of cluster dispersal under the influence of the pre-pulse in the $R_{i0} \le R_0 \le 5R_{i0}$ radius interval considered in this paper.

## References

[1] B.A. Remington, R.P. Drake, D.D. Ryutov. Rev. Mod. Phys., **78**, 755 (2006).

[2] Zs. Lecz, A. Andreev. PRR, **2**, 023088 (2020).

[3] A.A. Andreev, K.Yu. Platonov. JETP Lett., **112** (9), 550 (2020).

[4] A.A. Andreev, K.Yu. Platonov. Quantum Electron., **51**, 446 (2021).

[5] A.A. Andreev, K.Yu. Platonov, Zs. Lecz, N. Hafz. Sci. Rep., **11**, 15971 (2021). DOI: 10.1038/s41598-021-95465-x

[6] T. Fennel, K.-H. Meiwes-Broer, J. Tiggesbaumker, P.-G. Reinhard, P.M. Dinh, E. Suraud. Rev. Mod. Phys., **82**, 1793 (2010).

[7] M. Kalashnikov, A. Andreev, H. Schönnagel. AIP Conference Proceedings, **1228** (1), 175 (2010).

[8] K.B. Wharton, C.D. Boley, A.M. Komashko, A.M. Rubenchik, J. Zweiback, J. Crane, G. Hays, T.E. Cowan, T. Ditmire. Phys. Rev. E, **64**, 025401 (2001).

[9] A.A. Andreev, R. Sonobe, S. Kawata. Plasma Phys. & Control. Fusion, **48**, 1605 (2006).

[10] T. Ditmire, T. Donnelly, A.M. Rubenchik, R.W. Falcone, M.D. Perry. Phys. Rev. A, **53**, 3379 (1996).

[11] https://www.prism-cs.com/Software/Helios/overview.html

[12] M.V. Fedorov. J. Exp. Theor. Phys., **122**, 3, 449 (2016).

[13] https://github.com/Warwick-Plasma/epoch

[14] V.P. Krainov, M.B. Smirnov. Phys. Rep., **370**, 237 (2002). DOI: 10.1016/S0370-1573(02)00272-7

[15] A.A. Andreev, A.N. Semakhin, V.V. Akulinichev. Probl. Nauchn. Priborostr., **3**, 884 (1993).

[16] A.A. Andreev, K.Y. Platonov. Quantum Electron., **51**, 446 (2021).

[17] I. Kostyukov, J.-M. Rax. Phys. Rev. E, **67**, 066405 (2003).

[18] D.F. Zaretskii, F.F. Korneev, S.V. Popruzhenko. Quantum Electron., **37**, 565 (2007).

[19] M.B. Smirnov, V.P. Krainov. Laser Physics, **13**, 490 (2003).

[20] F. Brunel. Phys. Rev. Lett., **59**, 52 (1987).

[21] P. Gibbon, A.A. Andreev, K.Yu. Platonov. Plasma Phys. Control. Fusion, **54**, 045001 (2012). DOI: 10.1088/0741-3335/54/4/045001

*Translated by D.Safin*